Implicit Boundary Conditions for Direct Simulation Monte Carlo Method in MEMS Flow Predictions

W.W. Liou [1], **Y.C. Fang**[1]

Abstract: A simple implicit treatment for the low speed inflow and outflow boundary conditions for the direct simulation Monte Carlo (DSMC) of the flows in microelectromechanical systems (MEMS) is proposed. The local mean flow velocity, temperature, and number density near the subsonic boundaries were used to determine the number of molecules entering the computational domain and their corresponding velocities at every sample average step. The proposed boundary conditions were validated against micro-Poiseuille flows and micro-Couette flows. The results were compared with analytical solutions derived from the Navier-Stokes equations using first-order and second order slip-boundary conditions. The results show that the implicit treatment of the subsonic flow boundaries is robust and appropriate for use in the DSMC of the flows in MEMS.

keyword: DSMC, MEMS, boundary conditions, micro-Poiseuille flow, micro-Couette flow.

1 Introduction

The Micro-Electro-Mechanical system (MEMS) technologies have attracted a great deal of attention in different discipline areas. These devices are manufactured using processes similar to those used in the fabrication of microprocessors and promise the abilities to sense and to control physical processes with length scales in the order of a micron [Ho and Tai (1994)]. Potential applications for such devices can be found in a number of discipline areas, including chemical sensors, pressure sensors, and laminar flow control. Many of these proposed designs involve internal fluid flows, such as microchannel flows. A thorough understanding of the properties of such flows is important to the design, fabrication, and operation of MEMS.

In most MEMS flows, the mean free path of the fluid, λ, is of the same order as the characteristic system size, h. A ratio of the two length scales, λ/h, is commonly referred to as the Knudsen number, Kn. For many MEMS flows, the value of Kn is in the range of 0.1 to 10 and the fluid can no longer be approximated as a continuum. The fluid motions are better described from the molecular point of view, as opposed to the continuum point of view. The use of continuum-based techniques in MEMS flow analyses may therefore lead to large errors in the predictions.

[1] Western Michigan University, Kalamazoo, MI 49008, USA Department of Mechanical and Aeronautical Engineering.

The direct simulation Monte Carlo (DSMC) method of Bird(1994) is a well-developed technology. It is widely used for rarefied gas calculations and has been implemented in a parallel manner for high performance computation. This technique models a gas flow as thousands or millions of simulated "molecules", with each of them representing a large number of real gas molecules. As the simulated molecules move through the computational domain, they may collide with one another as well as with physical boundaries. The molecular properties are then sampled to determine the macroscopic flow quantities, such as the velocity and temperature. DSMC has also been applied successfully in the prediction of high speed flows in MEMS[Liou and Fang (2000)].

In a DSMC simulation, the numerical treatment of the boundaries of the computational domain is important. At the upstream boundary, the Dirichlet type of boundary conditions has usually been used. For a downstream or exit boundary, one traditional approach is to apply the uniform upstream flow condition at the downstream boundary. In this approach, which is often applied in the simulation of external flows, the downstream boundary is required to be far away from the base region. Another conventional approach is to impose a "vacuum" condition at the downstream boundary, where no molecules are allowed to enter the computational domain. These treatments of the flow conditions at the boundaries have been applied successfully in high speed flow calculations [Bird (1994), Liou and Fang (2000), Piekos and Breuer (1995)]. For low speed flows in atmospheric operating conditions, such as the flows in MEMS, these boundary conditions become inappropriate.

In a subsonic flow, the flow speed can be much lower than the most probable thermal speed. The boundary treatments mentioned above become physically unrealistic as they do not properly model the mass flux due to thermal fluctuations. It is important to take into account the necessary flow characteristic information at the boundaries of the computational domain for a subsonic flow. Although these issues are well known, methods to impose effectively boundary conditions for DSMC of low speed flows have not been as widely studied as those for continuum computational fluid dynamics (CFD). Piekos (1995) introduced particles based on the differences between a targeted number density and the values calculated by the ideal gas relations. Nance, etc.(1998) applied characteristics-based boundary conditions.

In this study, a new implicit treatment for the upstream and the downstream boundary conditions is proposed for the DSMC of low-speed micro-flows. Gas molecules are allowed to enter the flow domain from both the upstream inlet and the downstream exit boundaries. The number of the entering molecules, their velocities, and internal energies are determined by the local mean velocities, temperature, and number densities at the boundaries at every sample average step. The new implicit boundary condition formulations have been implemented in a DSMC code originally developed by Bird(1994). In this paper, some results of DSMC for micro-Poiseuille flows and micro-Couette flows are presented. For comparison, the DSMC results are also compared with continuum-based analytical solutions using the Maxwellian first-order and Beskok's (1996) second-order slip-boundary conditions.

2 New implicit boundary treatment

Microflows often operate with a given pressure (gradient) at the inlet and the outlet boundaries. The inlet velocity distributions are often not available due to experimental difficulties. In this section, the new implicit treatment for the low-speed inlet and exit boundaries for the DSMC of micro-flows in such operation conditions is described.

2.1 Implicit velocity distributions for entering molecules

For an equilibrium gas with a one-dimensional mean flow, the quantities associated with the molecules entering the computational domain from either the upstream inlet boundary or the downstream exit boundary can be determined according to the Maxwellian equilibrium distribution function,

$$f_0 = \frac{\beta^3}{\pi^{3/2}} \exp\left(-\beta^2 c'^2\right) \tag{1}$$

where

$$\beta = 1/\sqrt{2RT} \tag{2}$$

R denotes the universal gas constant, c' the thermal speed of molecule, and T gas temperature. Using the Maxwellian distribution function, the number flux of the molecules entering the computational domain can be calculated based on the local temperature and the mean flow velocity. At either the upstream or the downstream boundaries, the number flux, F_j, from a boundary cell j can be written as

$$F_j = \frac{n_j}{2\sqrt{\pi}\beta_j}\left[\exp\left(-s_j^2\cos^2\theta\right) + \sqrt{\pi}s_j\cos\theta\left\{1+\mathrm{erf}\left(s_j\cos\theta\right)\right\}\right] \tag{3}$$

where

$$s_j = U_j\beta_j \tag{4}$$

$$\beta_j = 1/\sqrt{2RT_j} \tag{5}$$

'erf' represents the error function, n_j the number density of molecules in cell j. T_j and U_j denote the local temperature and the streamwise mean velocity component, respectively. s_j denotes the molecular speed ratio and β_j is related to the thermal scattering. The value of θ is zero for the upstream boundary and π for the downstream exit boundary. The velocity components of the entering molecule can be determined by using the acceptance-rejection method [Bird (1994)] and the Maxwellian distribution function.

At the upstream inlet boundary, the streamwise thermal velocity, u', of the molecules entering the computational domain should be found in the interval $[-U_j, \infty)$, with a distribution function,

$$f_{u'} \propto \left(\beta u' + s_j\right)\exp\left(-\beta^2 u'^2\right) \tag{6}$$

To numerically implement the acceptance-rejection method using Eq. 6, the upper limit of ∞ is replaced by a cut-off value of $3C_{mp}$. C_{mp} represents the local most probable thermal speed of molecules, or,

$$C_{mp} = \sqrt{2RT_j} \tag{7}$$

In other words, the thermal velocity, u', is randomly sampled in the interval $[-u,\ 3C_{mp}]$. The resulting streamwise total velocity, $u = U_j + u'$, of the molecules entering the computational domain becomes

$$u = \left(U_j + 3C_{mp}\right)R_f \tag{8}$$

R_f represents a random fraction number. The two cross-stream velocity components are assumed to be of the following form,

$$v = A\cos\phi \tag{9}$$

$$w = A\sin\phi \tag{10}$$

The magnitude, A, lies between 0 and ∞, with a distribution function,

$$f_A = \exp\left(-\beta^2 A^2\right) \tag{11}$$

Using the acceptance-rejection method, the magnitude, A, can be written as

$$A = \sqrt{-\ln\left(R_f\right)}/\beta = \sqrt{-\ln\left(R_f\right)}C_{mp} \tag{12}$$

The angle, ϕ, is uniformly distributed between 0 and 2π. That is,

$$\phi = 2\pi R_f \tag{13}$$

Similarly, at a downstream exit boundary, the streamwise thermal velocity of the molecule entering the computational domain from downstream is set in the interval $[-3C_{mp},\ -U_j]$.

The resulting distributions of the velocity components for the molecule entering the computational domain become,

$$u = (U_j - 3C_{mp})\, R_f \tag{14}$$

$$v = A\cos\phi + V_j \tag{15}$$

$$w = A\sin\phi \tag{16}$$

where, V_j denotes the computed local mean transverse velocity. Eq. 3 can be used to obtain the net mass flux at a subsonic boundary with given mean velocity and temperature. In the following two sections, the methodologies to determine the mean quantities at the boundaries are described.

2.2 Downstream pressure conditions

As is mentioned earlier, it is often the pressure, instead of the velocity, that is given at the downstream exit boundary of microflows. A set of physically reasonable boundary conditions to determine the flow properties with a given pressure is needed. These boundary conditions at the exit are of critical importance to a successful DSMC simulation of microflows.

In continuum CFD, the downstream pressure condition in a subsonic, pressure-driven flow can be imposed by using the method of characteristics. Inspired by a characteristic theory used in continuum CFD [Whitfield and Janus (1984)], Nance, etc.(1998) proposed a set of correction equations for the pressure boundary conditions. We begin by applying the correction equations proposed by Nance, etc.(1998) for the flow properties at the exit boundary in the following form,

$$(\rho_e)_j^k = \rho_j^k + \frac{p_e - p_j^k}{\left(a_j^k\right)^2} \tag{17}$$

$$(u_e)_j^k = u_j^k + \frac{p_j^k - p_e}{\rho_j^k a_j^k} \tag{18}$$

$$(v_e)_j^k = v_j^k \tag{19}$$

$$(T_e)_j^k = P_e / \left[(\rho_e)_j^k R\right] \tag{20}$$

The subscript e represents quantities at the exit boundary, superscript k the computed quantities at the k-th time step, R the gas constant, and a_j^k the local exit speed of sound. p_e denotes the imposed pressure at exit. There is little details given in Nance, etc.(1998) regarding the implementation of the equations. The current implementation of the characteristics-based equations (17-20) ensures a proper account of the influx of mass from the exit boundary and the overall mass balance in the microchannels. The updated mean quantities are first determined by the following sample average equations

$$U_j = \frac{1}{N_j}\sum u \tag{21}$$

$$V_j = \frac{1}{N_j}\sum v \tag{22}$$

$$\rho_j = n_j m \tag{23}$$

$$T_j = \left(3T_{tr} + \xi_r T_{rot}\right) / \left(3 + \xi_r\right) \tag{24}$$

$$p_j = n_j K T_j \tag{25}$$

where T_{tr} denotes the translational temperature, T_{rot} the rotational temperature, and ξ_r the number of rotational degree of freedom. K represents the Boltzmann constant. The calculated mean quantities were then used in equations (17-20) to determine the number and the velocity distribution of the molecules required to enter the computational domain from the exit boundary. The current treatment of the pressure downstream boundary conditions consists of the following steps:

Step 1. Determine the number density of the molecules at the exit by

$$(n_e)_j = \rho_e / m \tag{26}$$

where m is the gas mass in the microchannel. A mass conservation is then satisfied in the computational domain.

Step 2. Determine the exit temperature by Eq. 20 and the corrected velocity components of the simulated molecules at the boundary cells using Eq. 18 and 19.

Step 3. Determine the exit mean flow velocity by sampling.

$$(U_e)_j = \frac{1}{N_j}\sum u_e \tag{27}$$

$$(V_e)_j = \frac{1}{N_j}\sum v_e \tag{28}$$

Step 4. The implicitly determined downstream properties can then be used to calculate the number of the entering molecules from the number flux function, Eq. 3, and their velocity components from the velocity distribution functions, Eq. 14-16.

2.3 Upstream mean flow condition

Several types of treatment have been proposed [Nance, etc.(1998), Ikegawa and Kobayashi (1990)] for the velocity at a subsonic upstream inlet boundary. In Ikegawa and Kobayashi (1990), the mean flow velocity $U(t)$ at the boundaries was determined based on the number of molecules flowing in, $N_{in}^{(t-\delta t)}$, and out, $N_{out}^{(t-\delta t)}$, from the upstream or the downstream boundaries at previous time,

$$U(t) = \frac{N_{in}^{(t-\delta t)} - N_{out}^{(t-\delta t)}}{n\,\delta t\, A} \tag{29}$$

where the molecule number N_{in} is

$$N_{in} = F\,\delta t\, A \tag{30}$$

δt represents a time step and A the boundary cross-section area. F denotes a number flux determined by averaging Eq. 3 over the whole inlet boundary. In a single time step, both $(n\delta t A)$

and $N_{in} - N_{out}$ are small and the scattering of may become rather large, causing the numerical solution to become unstable. Ikegawa and Kobayashi (1990) reduced the scattering by using the average value of two consecutive time steps.

The inflow mean velocity condition used in Nance, etc. (1998) is quite similar to that proposed by Ikegawa and Kobayashi (1990). In stead of using a constant mean flow velocity, the particle conservation was applied on a per-cell basis. The particle fluxes were computed from the Maxwellian distribution. In contrast, Ikegawa and Kobayashi determined the particle fluxes by the actual particle counts across the computational boundaries.

A rather simple implicit type of condition is proposed in this paper for the mean flow velocity at the upstream inlet. A first-order extrapolation is used to determine the inlet mean velocity from inside the computational domain. That is,

$$(U_{in})_j = U_j \tag{31}$$

The term on the right side is the cell-average velocity of the upstream boundary cells, which can be calculated from Eq. 21. This method is commonly used in continuum CFD and has been found successful for a wide range of internal as well as external flows. The inflow temperature, T_{in}, and number density, n_{in}, can then be obtained from the given pressure, p_{in}, and density, ρ_{in}, according to the conservation of mass and the equation of state. That is,

$$(n_{in})_j = \rho_{in}/m \tag{32}$$

$$(T_{in})_j = p_{in}/\rho_{in}R \tag{33}$$

The particle number fluxes and the velocity components of entering molecules were determined locally from the Maxwellian distribution.

3 Microflow predictions

The new implicit boundary treatment has been implemented into a DSMC code. The original version of the code was developed by Bird(1994). The modified DSMC code has been applied to calculate two types of microscale flows, the micro-Couette flow and the micro-Poiseuille flow shown in Fig. 1. Some of the computational results are presented and compared with the analytical results based on the Navier-Stokes equations with velocity-slip boundary conditions.

For fully developed parallel flows with low Reynolds numbers, the Navier-Stokes equations can be simplified,

$$\frac{dp}{dx} = \mu \frac{d^2u}{dy^2} \tag{34}$$

For the micro-Couette flow, the pressure gradient is zero and the upper plate moves at a speed of U. A slip boundary condition at the wall proposed by Maxwell can be written as,

$$u - u_w = \frac{2-\sigma_v}{\sigma_v} Kn \frac{du}{dy} \tag{35}$$

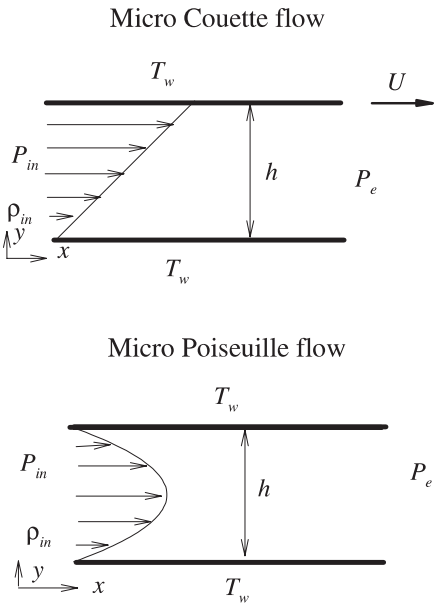

Figure 1 : Simulated micro-geometries.

This is considered first order in Kn. A second-order slip boundary condition has been proposed in Beskok (1996),

$$u - u_w = \frac{2-\sigma_v}{\sigma_v} \frac{Kn}{1+Kn} Kn \frac{du}{dy} \tag{36}$$

A distribution of the mean flow velocity, u, for the micro-Couette flow can be obtained by solving Eq. 34 and 35, which gives,

$$\frac{u}{U} = \frac{1}{2\left(\frac{2-\sigma_v}{\sigma_v}\right) Kn + 1} \left(\frac{y}{h} + \frac{2-\sigma_v}{\sigma_v} Kn \right) \tag{37}$$

Eq. 37 shows that, according to this continuum-based model, the Kn of the microflow determines the slop of the velocity profile and the slip velocity on the walls. Note that a use of the second-order slip condition would result in the same velocity distribution as Eq. 37 due to the linear nature of the velocity profile [Beskok (1996)].

For a pressure-driven micro-Poiseuille flow, the use of the first-order slip boundary condition results in the following distribution for the mean velocity.

$$u = \frac{h^2}{2\mu} \frac{dp}{dx} \left[\left(\frac{y}{h}\right)^2 - \frac{y}{h} - \frac{2-\sigma_v}{\sigma_v} Kn \right] \tag{38}$$

By using the second-order slip boundary condition, Eq. 36, one would obtain a more accurate distribution for the velocity,

$$u = \frac{h^2}{2\mu} \frac{dp}{dx} \left[\left(\frac{y}{h}\right)^2 - \frac{y}{h} - \frac{2-\sigma_v}{\sigma_v} \frac{Kn}{1+Kn} \right] \tag{39}$$

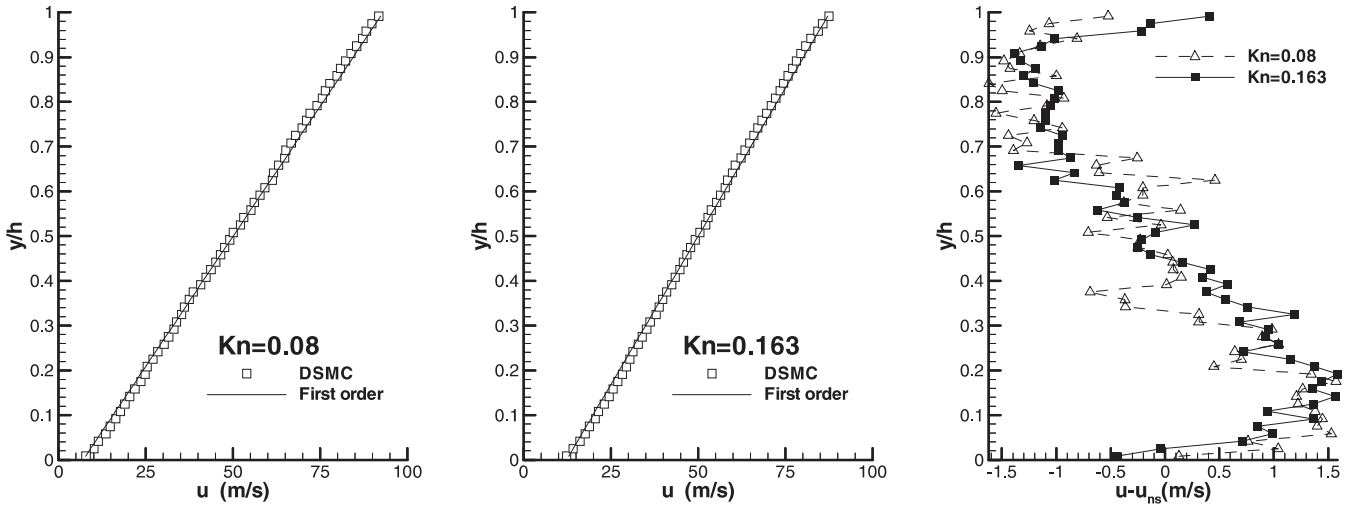

(a) (b) (c)

Figure 2 : Comparison of the velocity profiles for micro-Couette flows. (a) $Kn = 0.08$; (b) $Kn = 0.163$; (c) Velocity difference between the present DSMC and the continuum-based solutions.

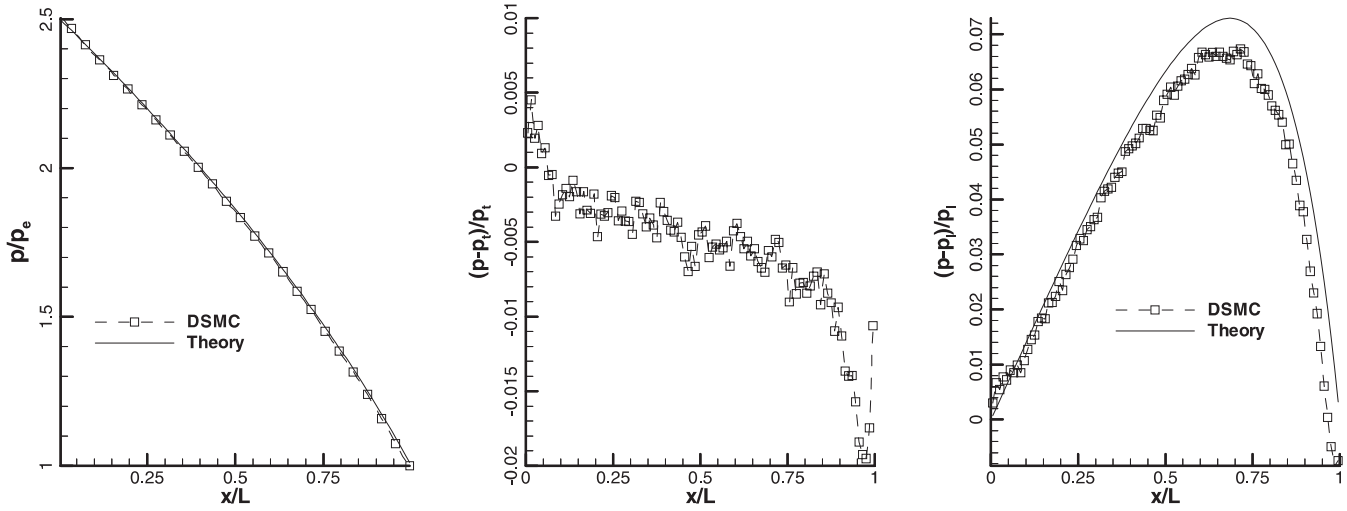

(a) (b) (c)

Figure 3 : Comparison of pressure distributions of micro-Poiseuille flow, Case 1. (a) Comparison of pressure distributions; (b) Relative errors of pressure distribution; (c) Deviations from linear pressure drop.

Both Eq. 38 and 39 show that the velocity is a function of the local Knudsen number, the distance to the wall, as well as the pressure gradient. For a full diffusely reflecting wall, $\sigma_v = 1$, nondimensional forms of Eq. 38 and 39 can be obtained by using the centerline velocity as the velocity scale. The resulting nondimensional forms of the first-order and the second-order accurate velocity profiles are, respectively,

$$\frac{u}{u_c} = \left[-\left(\frac{y}{h}\right)^2 + \frac{y}{h} + Kn \right] \Big/ \left(\frac{1}{4} + Kn \right) \tag{40}$$

$$\frac{u}{u_c} = \left[-\left(\frac{y}{h}\right)^2 + \frac{y}{h} + \frac{Kn}{1+Kn} \right] \Big/ \left(\frac{1}{4} + \frac{Kn}{1+Kn} \right) \tag{41}$$

In the slip-flow range with Kn less than 0.1, the continuum-based solution approximates well the microflows and is com-

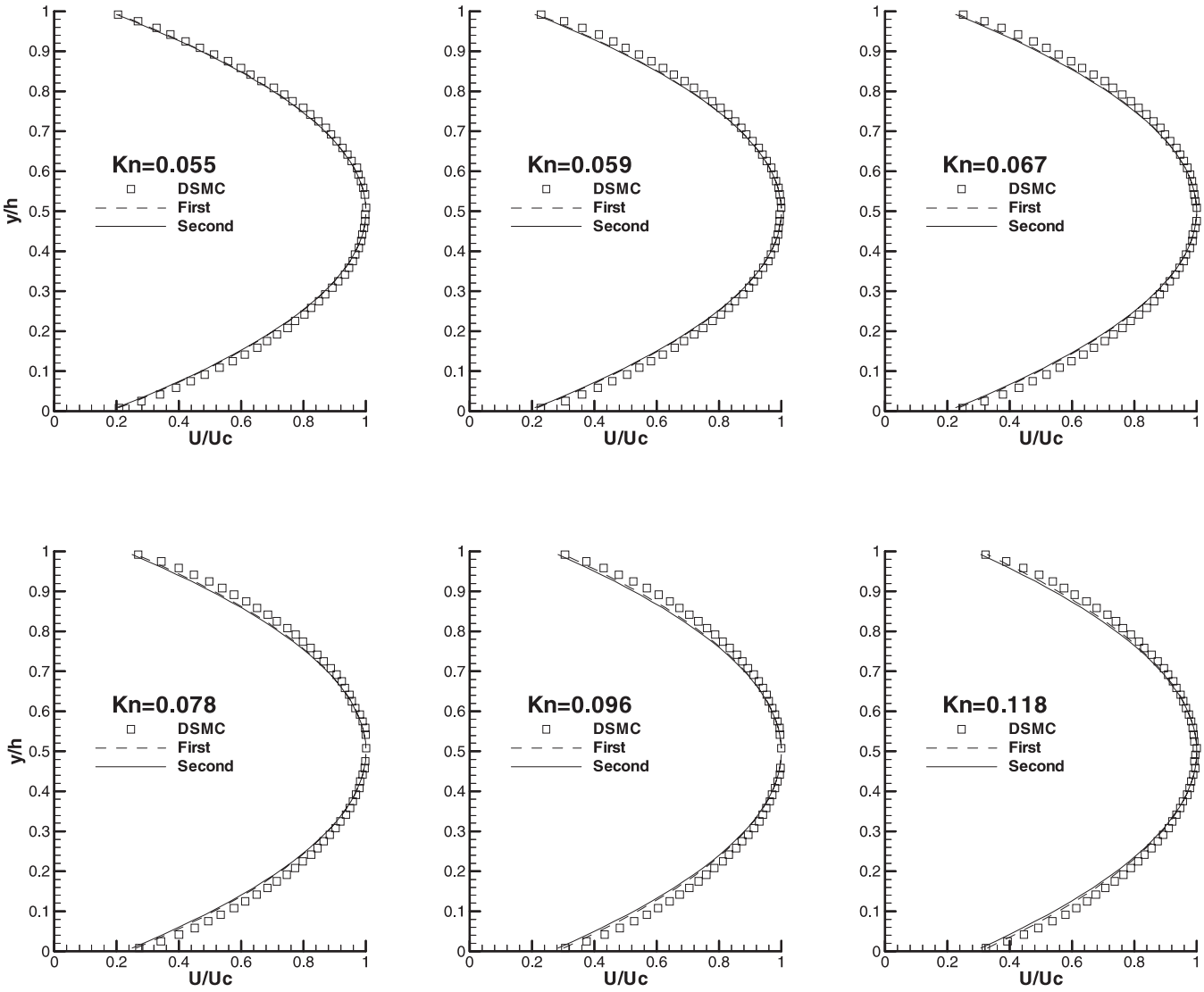

Figure 4 : Comparison of velocity profiles of micro-Poiseuille flow, Case 1.

monly used for comparison with DSMC results.

4 Results and discussions

In this section, the predicted micro-Couette flows and micro-Poiseuille flows are presented. The results were obtained by using a DSMC solver and the new implicit treatment of the upstream and downstream conditions. For comparison, analytical solutions based on the Navier-Stokes equations and the slip flow boundary conditions are also presented.

4.1 Micro Couettef flow

For the simulated micro-Couette flow of Nitrogen, there is no pressure gradient and the pressure at the inlet and the outlet boundaries are both set at 0.83 atm ($p_e = p_{in} = 0.83\,atm$). The inlet flow temperature, T_{in}, and the temperature of the upper and the lower walls, T_w, are all set equal to 300 K. The upper wall moves with a speed of 100 m/s. Two cases were simulated. The channel heights are 0.4 μm and 0.8 μm, respectively. The Knudsen numbers, based on the channel height and the inlet condition are 0.08 and 0.163. Rectangular cells (100×60) were used in the computational grid for both cases. The simulated number of molecules is about 320,000. Runs

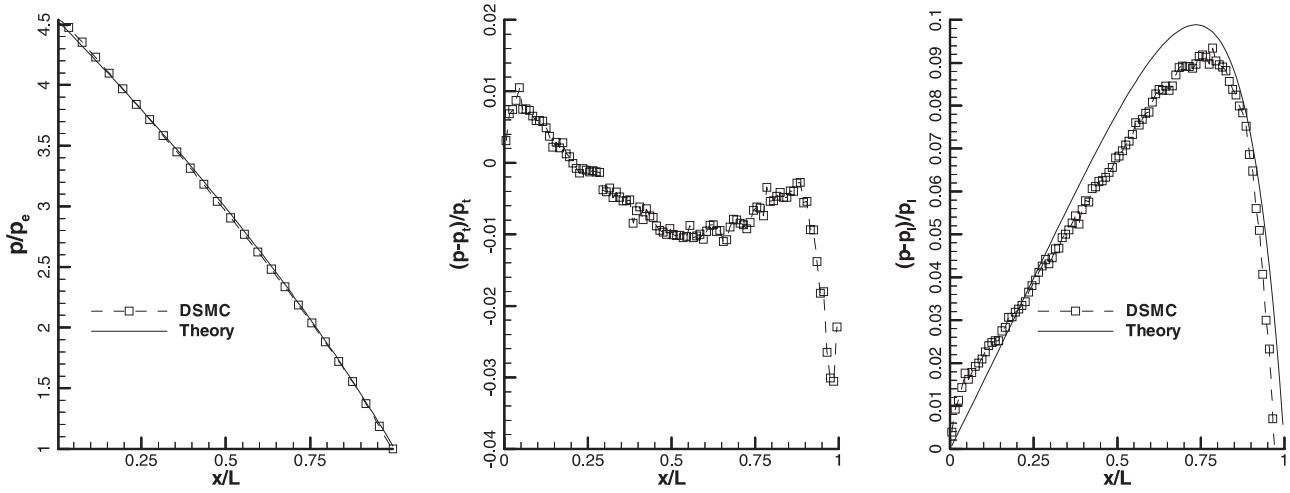

(a) (b) (c)

Figure 5 : Comparison of pressure distributions of micro-Poiseuille flow, Case 2. (a) Comparison of pressure distributions; (b) Relative errors of pressure distribution; (c) Deviations from linear pressure drop.

on SGI-Octane typically took roughly 48 hours of CPU time.

Fig. 2(a) and 2(b) show the predicted velocity profiles for $Kn = 0.08$ and $Kn = 0.163$, respectively. The corresponding linear profiles given in Eq. 37 are also shown for comparison. Overall, there is a good agreement between the continuum-based solutions and the DSMC results for $Kn = 0.08$, which suggests that the current implicit boundary condition is suitable for DSMC. In the center portion of the channel, the DSMC solution agrees well with the continuum-based linear solution. There appears to be a slight difference between the two solutions away from the center portion. For the case with a higher Kn (0.163), a nonlinear profile was obtained by the DSMC. Compared with the linear, continuum-based solution, the DSMC method has predicted a velocity profile with a lower value of slope in the center portion of the channel and with slight curvatures approaching the wall. Fig. 2(c) shows the velocity differences between the DSMC results and the continuum-based analytical solutions across the channel for both cases. The nonlinear, wavy behavior of the DSMC solution is evident, specially for the higher Kn case. The effect of Kn on the micro-Couette flow observed in the present DSMC results has not been reported in prior published articles that we are aware of. The difference in the wall slip velocity between the DSMC and the analytical solution is small. For the higher Kn case (0.163), the calculated slip velocity at the lower wall, 11.87 *m/s*, is roughly 3% lower than that of Eq. 37. It suggests that the difference between the velocity profiles predicted by the present DSMC method and the analytical form based on the continuum assumption is not necessarily due entirely to the low-order of accuracy in the slip-boundary condition.

4.2 Micro Poiseuille flow

Two micro-Poiseuille flows were calculated. The value of the local Kn in the channels for Case 1 varies between 0.055 and 0.123 and between 0.19 and 0.72 for Case 2. The height of the micro-channel, h, is 0.4 μm for both cases. The pressure ratios are 2.5 for Case 1 and 4.54 for Case 2. The computation grid contains 100×60 rectangular cells. The simulated number of molecules is about 180,000. Runs on SGI-Octane typically took nearly 36 hours of CPU time.

Fig. 3(a) shows the predicted pressure distribution along the channel centerline for Case 1. A continuum-based analytical form obtained using the first-order slip condition [Piekos(1995)] was also included for comparison. Fig. 3(b) shows the relative difference of pressure between the DSMC result and the analytical solution. The maximum difference is roughly 2%, indicating that the current boundary treatment is appropriate to use with the DSMC techniques. Both methods predicted pressure that are nonlinearly distributed along the channel, which has been observed experimentally for microchannel flows. Fig. 3(c) compares the deviations of the DSMC and of the analytical pressure drops from the linear distribution, p_l. The nonlinearity exhibited by the DSMC solution is 0.5% lower than that of the continuum-based solution.

Fig. 4 shows a comparison of the DSMC velocity profiles with

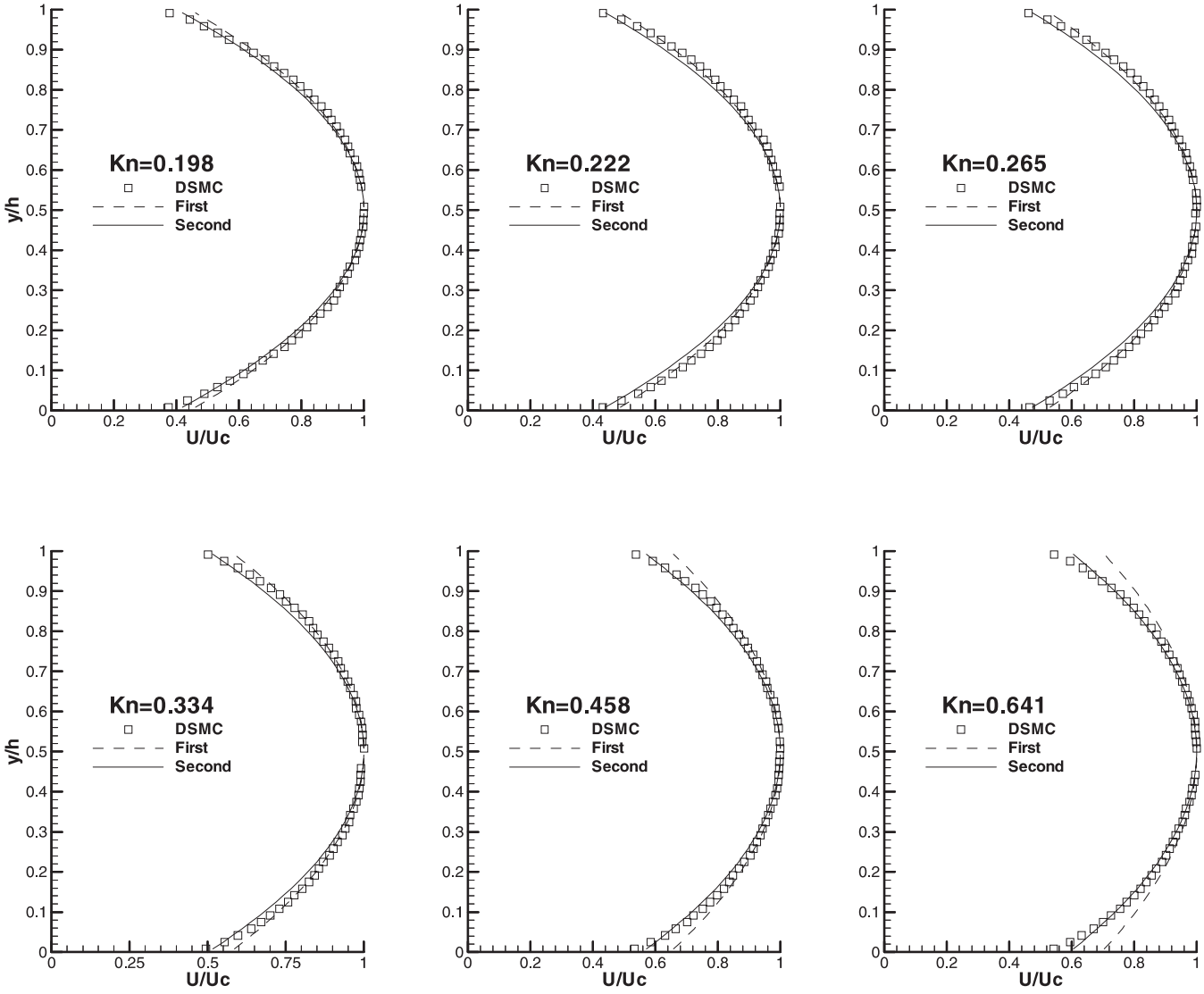

Figure 6 : Comparison of velocity profiles of micro-Poiseuille flow, Case 2.

the continuum-based analytical solution of Eq. 40 and 41 at six different locations along the channel. The value of the Kn changes from 0.055 to 0.118. For the small Kn, there is little difference between the first- and the second-order accurate continuum-based velocity profiles. The calculated profiles agree well with the continuum solutions for all the stations compared. In this low Kn range, the continuum-based analytical result provides an approximated solution to the microflow considered. The results show that the present implicit treatment of the upstream and the downstream boundary conditions is consistent with the DSMC procedure and has produced accurate numerical predictions to the microflows considered.

For Case 2, the pressure ratio is 4.54, compared with 2.5 for Case 1. The local Kn are higher than Case 1. Fig. 5(a) shows the pressure distribution along the centerline of the channel. Fig. 5(b) shows the difference of pressure distribution between the DSMC solutions and the continuum-based form, with a maximum difference of 3%. Compared with Case 1, a stronger nonlinearity is predicted by both methods. Fig. 5(c) shows that the deviation from the linear distribution is 9% for the DSMC results and 10% for the continuum-based results.

Fig. 6 shows the calculated mean velocity profiles at six different stations along the channel. Continuum-based solutions using the first-order and the second-order slip-wall conditions were also included for comparison. The differences between the first-order profiles and the second-order profiles for this

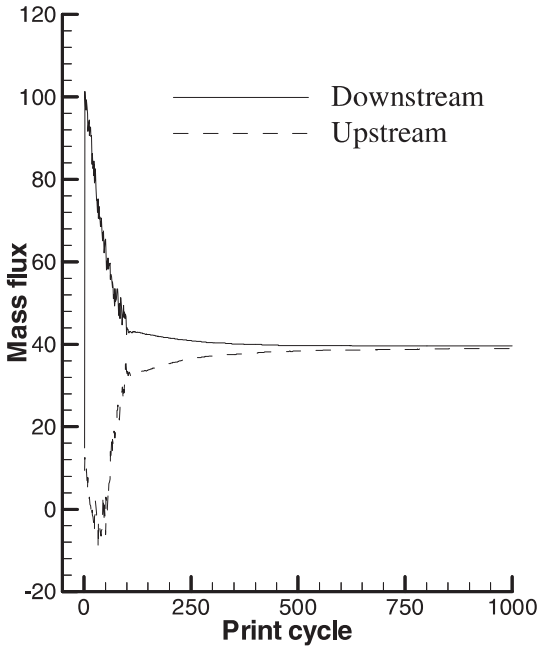

Figure 7 : Evolution of mass fluxes at the upstream and the downstream boundaries, Case 2.

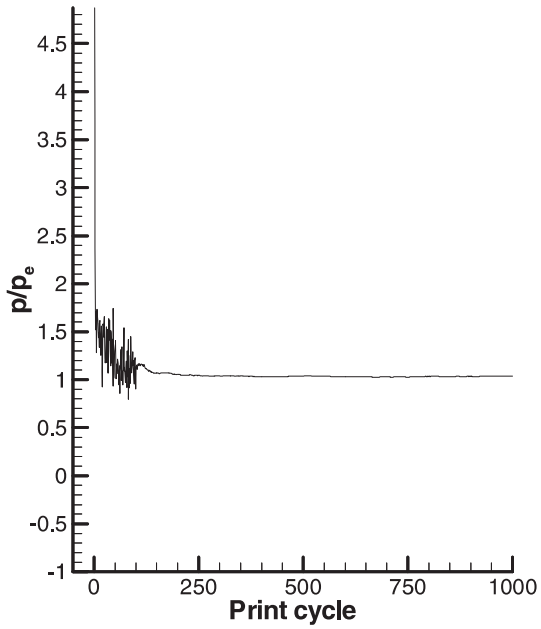

Figure 8 : Evolution of the downstream pressure, Case 2.

case are more significant than those for Case 1. While the second-order profiles give reasonable approximations to the DSMC results for Kn up to 0.641, the first-order profiles move away from the DSMC results as the value of the Kn increases, with the highest difference occurring at the channel wall.

Fig. 7 shows the evolution of the mass fluxes at the upstream and the downstream flow boundaries as the solution progresses for Case 2. After an initial transient from the uniform initial conditions set for the entire computational domain, the mass fluxes converge and a mass balance in the channel is established. Fig. 8 shows the variation of the pressure at the downstream boundary, nondimensionalized by the imposed exit pressure, p_e, during the same print cycle. Again, the pressure converges to the imposed value after a transient variation from the uniform initial conditions. Fig. 7 and 8 show that the present implicit treatment of the low-speed boundaries supports a stable and converging solution process for the DSMC of micro-flows.

As is mentioned earlier, boundary conditions previously developed for the DSMC of high-speed flows do not properly model the mass flux due to thermal fluctuations in flows of low-speed. Fig. 9(a) shows the distribution of the influxes of fluid mass into the computational domain due to the thermal fluctuations, $\overline{nmu}$, at the upstream and the downstream boundaries for the two micro-Poiseuille flows. The distributions have been nondimensionalized by the local mean mass flux. Since the number flux at the boundaries was determined by the local mean properties, the local thermal mass fluxes are not uniformly distributed across the channel. According to the present results, however, the nonuniformity does decrease at higher Kn (Case 2). The sectional thermal mass fluxes obtained by integrating the thermal mass flux over the inlet and the outlet boundaries are shown in Fig. 9(b). At the upstream boundary, the thermal mass flux into the computational domain increases with pressure gradient due to the increased mean velocity. At the downstream boundary, the influx of fluid mass due to thermal fluctuations is nearly 50% of that of the total mass flux for Case 1 and 20% for Case 2. The results show that the thermal mass flux entering the flow domain at a downstream boundary is significant and the "vacuum" boundary condition used for high-speed flows is not physically reasonable to use in the DSMC of the subsonic micro-flows in MEMS.

5 Concluding remarks

A new implicit treatment of the boundary conditions for the DSMC of low-speed MEMS flows has been presented. The local mean flow velocity, temperature and number density near the boundaries were used to determine the number of molecules entering the computation domain and their corresponding velocities. The pressure exit condition has been physically imposed. The method enforces mass conservation and is consistent with the characteristic theory of subsonic flows.

Micro-Couette flows and micro-Poiseuille flows were computed and compared with analytical solutions derived from the Navier-Stokes equations using slip-boundary conditions. The results show that the proposed implicit treatment of subsonic

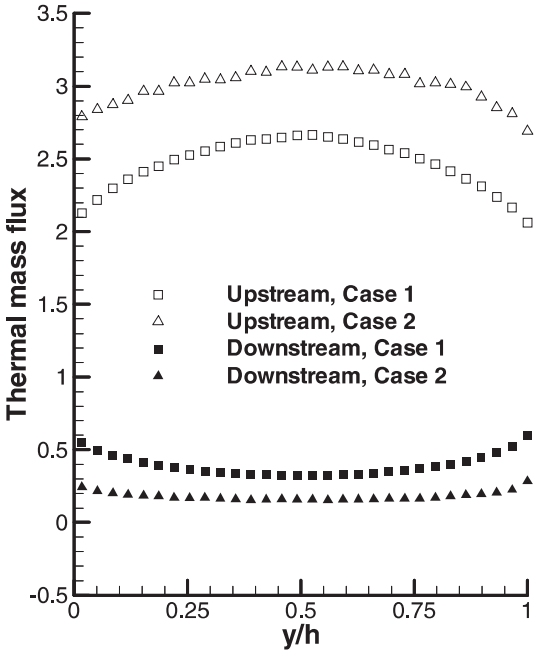

(a)

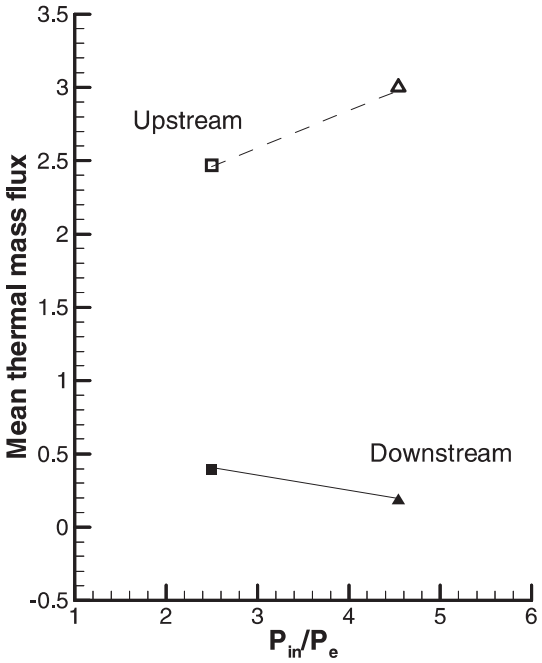

(b)

Figure 9 : Thermal mass flux nondimensionalized by mean mass flux for micro-Poiseuille flows. (a) local thermal mass influx; (b) sectional mean thermal mass influx.

flow boundaries is robust and appropriate for use in the DSMC of the flows in MEMS.

The DSMC results indicate that the velocity profile of the micro-Couette flow exhibits a nonlinear wavy behavior that has not been reported previously.

The results also show that the mass influx due to thermal fluctuations represents a significant portion of the overall mass flux balance in subsonic MEMS flows.

References

Beskok, A. (1996): *Simulations and Models for Gas Flows in Microgeometries*. Ph.D. Thesis, Princeton University, 2062-T.

Bird, G. A. (1994): *Molecular Gas Dynamics and the Direct Simulation of Gas Flows*. Oxford Science Publications.

Ho, C. M.; Tai, Y. C. (1994): MEMS: Science and technology. In *Application of Microfabrication to Fluid Mechanics*, pp. 39–49. ASME.

Ikegawa, M.; Kobayashi, J. (1990): Development of a rarefied flow simulator using the direct-simulation Monte Carlo method. *JSME International Journal*, vol. 33, no. 3, pp. 463–467.

Liou, W. W.; Fang, Y. C. (2000): Heat transfer in microchannel devices using DSMC. *Journal of Micoelectromechanical Systems. (submitted)*.

Nance, R. P.; Hash, D. B.; Hassan, H. A. (1998): Role of boundary conditions in Monte Carlo simulation of MEMS devices. *Journal of Thermophysics and Heat Transfer*, vol. 12, no. 3, pp. 447–449.

Piekos, E. S.; Breuer, K. S. (1995): DSMC modeling of micromechanical devices. In *AIAA*. paper 95-2089, SanDiego, CA. June 19-22.

Whitfield, D. L.; Janus, J. M. (1984): Three-dimensional unsteady Euler equations solution using flux vector splitting. In *AIAA*. Paper 84-1552.